SAE INTERNATIONAL®

Gas Exchange and Injection Modeling of an Advanced Natural Gas Engine for Heavy Duty Applications

2017-24-0026
Published 09/04/2017

Davide Paredi, Tommaso Lucchini, Gianluca D'Errico, and Angelo Onorati
Politecnico di Milano

Stefano Golini and Nicola Rapetto
FPT Industrial SpA

CITATION: Paredi, D., Lucchini, T., D'Errico, G., Onorati, A. et al., "Gas Exchange and Injection Modeling of an Advanced Natural Gas Engine for Heavy Duty Applications," SAE Technical Paper 2017-24-0026, 2017, doi:10.4271/2017-24-0026.

Abstract

The scope of the work presented in this paper was to apply the latest open source CFD achievements to design a state of the art, direct-injection (DI), heavy-duty, natural gas-fueled engine. Within this context, an initial steady-state analysis of the in-cylinder flow was performed by simulating three different intake ducts geometries, each one with seven different valve lift values, chosen according to an estabilished methodology proposed by AVL. The discharge coefficient (C_d) and the Tumble Ratio (TR) were calculated in each case, and an optimal intake ports geometry configuration was assessed in terms of a compromise between the desired intensity of tumble in the chamber and the satisfaction of an adequate value of C_d. Subsequently, full-cycle, cold-flow simulations were performed for three different engine operating points, in order to evaluate the in-cylinder development of TR and turbulent kinetic energy (TKE) under transient conditions. The latest achievements in open source mesh generation and motions were applied, along with time-varying and case-fitted inizialization values for the fields of intake pressure and temperature. Finally, direct-injection of natural gas in the cylinder was incorporated in full-cycle simulations, to evaluate the effects of injection on charge motions and charge homogeneity at the estimated spark timing. Three specific engine operating points were simulated and different combinations of turbochargers and valve lift laws were tested. Results consistency was verified by means of validations with data from 1D simulations and literature.

Introduction

In recent years, regulations [1] concerning internal combustion engines (ICE) emissions in terms of particulate, carbon oxides (CO, CO_2) and NO_x became more and more stringent, fact which lead to research activities aimed at the utilization of gaseous fuels as a viable alternative. Initially, most of the interest was directed towards H_2 [2] and its application in ICE has been intensively researched through the years [3, 4]. However, disadvantages such as the difficulties related to its production phase allowed for natural gas (NG) to become a more viable option which has been recently exploited. It was demonstrated that NG-fueled engines proved to be capable to meet even the most recent emission requirements [5, 6, 7], mainly thanks to the low carbon/hydrogen ratio of the methane compared to conventional combustibles; furthermore gaseous fuels such as CH_4 and its derivatives have the advantage to be potentially produced by renewable resources. During the last decade, researches were focused on the performances of gasoline spark ignition (SI) engines converted for a NG-based use [8] and results have been encouraging, since the high octane number [1] of NG allows for higher values of compression ratio as well as leaner mixtures, thus leading to increased engine efficiencies if compared to what is possible to achieve under conventional fuels [9]. The combination of low emissions and high efficiencies allows NG to be considered as a valid alternative fuel for heavy-duty transport applications. It is under these circumstances that the HDGas project was developed, consisting in the design of an all-new NG-fueled heavy-duty engine. It must be reported that a drawback which is in common for all the gaseous fuels consists in an implicitly low volumetric efficiency, which would lead to a low engine power density if the gas was to be injected indirectly in the combustion chamber by means of traditional port-fuel injectors (PFI). A solution to this problem is represented by the use of direct fuel injection (DFI), which is also fundamental to avoid the risk of combustion problems such as knock and backfire, and, consequently, to pursue the reduction of emissions and the increment of efficiency. DI also allows for a higher degree of control of the mixture formation process in the chamber thus leading to an optimal charge stratification, which is a factor of high importance in order to guarantee a correct flame propagation [10] under lean mixture conditions for turbocharged engines.

Under fast-paced evolution and stringent emission regulations, Computational Fluid Dynamics (CFD) is nowadays widely applied for operations of ICE design, test and development. Within the context of the HDGas project, CFD was extensively used to design the intake ports, identify the proper valve timing and study the

combined effects of charge motions and injection on the fuel-air mixing process. Modeling of fuel injection is one of the most challenging tasks in CFD simulations: in case of liquid fuels accurate sub-models for atomization, break-up and evaporation of the spray are needed, while the gaseous injection, despite not requiring such sub-models, still remains a complex task since the flow within the injector is supersonic and, for high values of the ratio between injection pressure and ambient pressure, the jet structure at the nozzle becomes complex, showing underexpansion effects and pressure shocks under the form of Mach Disks. During the last decade, in literature gaseous jet underexpansion has been experimentally investigated using hydrogen [11, 12], while recently CFD simulations validatiing high-pressure gaseous injection conditions were performed for single hole and multi-hole injectors [13], with the aim of analyzing the effects of different injection and ambient pressure values, as well as evaluating the accuracy of the predicted gas dynamic and air-fuel mixing process compared to experimental data [14, 15]. The correlation between numerical results and different grid specifications along with multiple injection conditions was also matter of extended research [16]. On the basis of such theoretical aspects, the work proposed in this paper represented an important task, due to the need to achieve accurate results in a relatively small amount of time as a consequence of the tight industrial project schedule. One of the most important and innovative aspects of the work reported in this paper consisted in the fact that the process of design and development of a modern, heavy-duty, direct injection natural gas engine was carried out exclusively by means of CFD simulations. The achieved results were indeed used as main guidance and indication for the production of the first engine prototype, fact which highlights the degree of accuracy reached nowadays by CFD calculations. In particular, steady-state flow bench simulations were initially performed to design intake ducts capable to guarantee acceptable values of both flow coefficient and tumble ratio. Afterwards, the reference cylinder head layout was tested by means of cold-flow simulations for different engine operating conditions, in order to assess if adequate levels of the turbulent kinetic energy and intensity of tumble were reached. Finally, the full-cycle, cold-flow simulations were coupled with the direct injection of natural gas to verify that the air-fuel mixing process and the homogeneity of the charge satisfied the expected requirements, to ensure a stable and efficient combustion process under different operating conditions.

Numerical Modeling

The chosen CFD code and the processes of mesh generation are going to be described in the following section.

Description of the Chosen CFD Code

CFD simulations were carried out using the LibICE code, which is based on the OpenFOAM® (OF) technology and was extensively validated in past works against experimental data related to in-cylinder charge motions and fuel-air mixing during a full-cycle [17, 18, 19, 20, 21]. The simulations were performed using the RANS approach for turbulence modeling. Such a choice was mainly justified by the fact that RANS calculations currently offer the best compromise between required computational time and accuracy of results. However, nowadays the LES approach [22, 23] is also used in the field of natural gas injection modeling.

Steady-State Flow Bench Simulations: Meshing Procedure

Each mesh which was used for the steady-state flow bench simulations was created with cfMesh®, an open source generator which can be fully implemented in OpenFOAM. Such a software guaranteed an automatic generation of 3D meshes containing hexahedra and split-hexahedra, while also allowing the user to generate boundary layers on wall surfaces and to locally refine regions of interest in the computational domain. A range of 0.052 - 0.275 was chosen for the considered valve lift to diameter ratio values and 8 different lifts were tested. For any configuration, the computational mesh has approximately 1.4 million cells with a maximum cell size of 2.5 mm and the valve patches were properly refined up to 0.125 mm. Since the *standard k-ε* with scalable wall functions approach was used, the boundary layer was set to be one-cell thick.

Cold-Flow Simulations: Meshing Procedure

Fig.1 shows the approach which was considered for the execution of the proposed full cycle, cold-flow simulations. A stereolithography (STL) file for the engine geometry must be provided, with the piston at top dead center (TDC) and both intake and exhaust valves placed at a specific minimum lift value (which was chosen to be equal to 0.25 mm in this work). Firstly, the topology of the default STL file gets changed in order to match the desired crank angle (CA) engine position; afterwards, an hexahedral, body-fitted mesh is generated by means of the snappyHexMesh utility. The grid is successively deformed until the quality parameters of the mesh are satisfied; once such a constraint is not respected anymore, a new mesh is generated for that specific crank angle value and the whole process is executed from the beginning. As a consequence, under this approach a multiple number of meshes is employed, with each one of them valid for a certain crank angle interval. The motion of the internal grid points is automatically accomodated on the basis of the Laplace equation, according to the prescribed boundary motion technique already presented and validated in literature [24, 25].

Furthermore, as shown in Fig.2 the user has a high degree of control over the mesh quality, since actions such as boundary layer insertion and specific internal domain refinement are allowed. The maximum adopted cell size in the whole computational domain was equal to 2 mm, while the refined zone at the intake seats was chosen to be 1 mm in size. A set consisting in one boundary layer for each engine wall was specified, while the valves patches were refined up to 0.125 mm.

As it is displayed in Fig.3, for the full cycle cold-flow simulations (with and without gas injection) a strategy to change the reference STL file according to the specific engine phase was adopted. This choice allowed to consistently save on the total number of cells, since the parts of the engine domain which were not useful during the simulation (for example, the exhaust ducts during the intake phase) were removed. It must be noticed, however, that such a kind of strategy can only be applied for the simulation of one engine cycle.

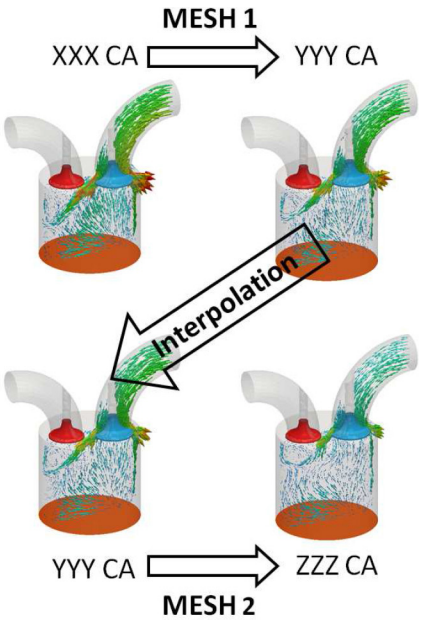

Figure 1. Moving mesh strategy for cold-flow simulations

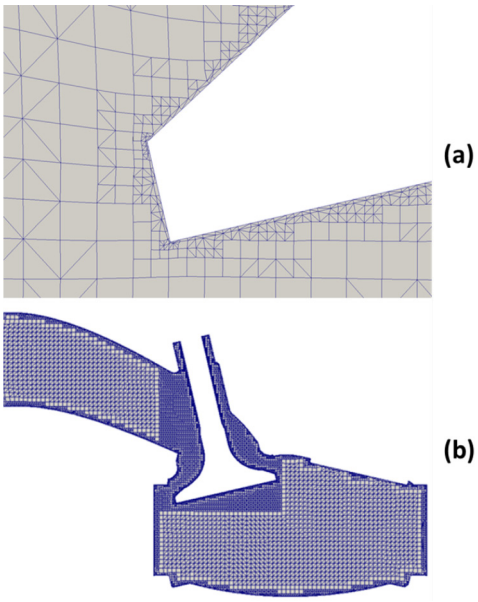

Figure 2. Examples of boundary layer (a) and specific internal refinement (b) created with the snappyHexMesh utility

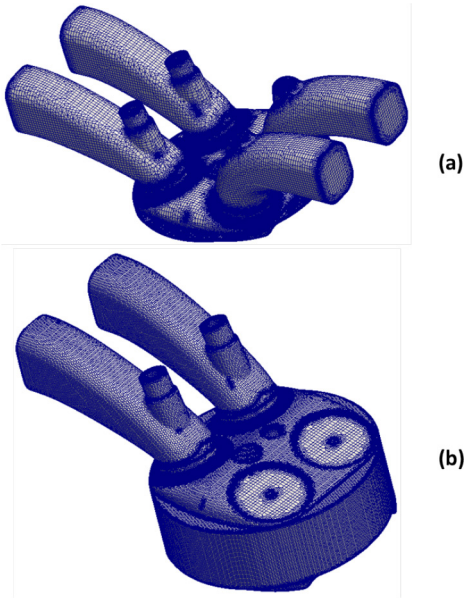

Figure 3. Examples of STL files respectively used for the overlap (a) and the intake (b) phase

Results

The design of the heavy-duty engine for the HDGas project was carried out by means of the OpenFOAM CFD code in three main phases:

1. As a first step, the initial configuration for the intake ducts of the engine was evaluated on the basis of its capability to provide a good compromise between generated tumble and flow discharge coefficient. The simulations were performed using air as working fluid and assuming it as incompressible. On the basis of the computed results, it was possible to design new engine configurations and simulate them as well;
2. The best set-up from the steady-state analysis was chosen and used as part of the final engine layout (intake and exhaust ducts, cylinder head and piston shape). A series of different engine operating points, at both partial and full-load conditions, were tested by means of transient cold-flow, full-cycle simulations. Different valve lift laws were tested as well. Specifically, the purpose of these computations was to assess the in-cylinder tumble motion and turbulent kinetic energy development for the real engine operating conditions which were considered as the most relevant (partial load, maximum torque and maximum power respectively). The chosen fluid was a mixture of air and a fraction in mass of the exhaust gases (EGR). The EGR values were specifically provided for each engine operating point;
3. The final step of the design process consisted in the evaluation of the effects of fuel injection over the charge motion, as well as the efficiency of the air-fuel mixing process and the level of mixture homogeneity inside the engine chamber. To perform such a task, the transient, full-cycle simulations with mesh motion were coupled with the high pressure injection of natural

gas. Computations proved to be extremely demanding in both time and resources, and an optimal compromise was required to be found between an accurate simulation of the injection phase (characterized by lower time-steps and a highly refined mesh) and the necessity to achieve results in a reasonable amount of time. Two partial load engine operating points were tested, as well as the full-load condition under two different intake valve lift laws.

Steady-State Flow Bench Simulations

The proposed work focused on applying CFD to design a direct injection, natural gas engine. Most of the current natural gas engines either are derived from the conversion of already existing CI units or they deploy port-fuel injection systems [26], while the goal of the HDGAs project was to develop a dedicated natural gas, direct-injection unit. As a consequence, a pent-roof layout was chosen for the combustion chamber, optimizing the aspects related to the cylinder filling as well as to the combustion efficiency, compared to what is possible to achieve with CI-derived flat chambers. Moreover, a pent-roof solution optimizes the use of four valves per cylinder, promoting a fast propagation of the flame front as well as allowing for a higher resistance to knock phenomena. Being the HDGas a heavy-duty engine, it was fundamental to investigate full-load operating conditions, for which the proper filling of the cylinder and a stable combustion process have to be ensured. For such reasons, the steady-state flow bench simulations focused on the evaluation of parameters such as the *Flow Coefficient* (c_d) and the *Tumble Ratio (TR)*. The former will always be presented in this paper in a normalized form.

Fig.4 reports the three different engine layouts which were tested under steady-state flow bench conditions. The intake ducts geometry (a) is what was initially provided by the manufacturer, while layouts (b) and (c) represent the modifications which were subsequently carried out on the basis of the results provided by the reported CFD simulations. Layout (b) is characterized by ducts with a larger section, in order to enhance the mass flow rate, as well as with a more axial orientation. Layout (c) on the other hand displays intake ducts which are more oriented towards the opposite cylinder wall, as it was initially chosen for the geometry (a), but an increase of the flow cross sectional area is visible nearby the caps of the valves stems.

The flow coefficient was evaluated according to Eq.1:

$$c_d = \frac{\dot{m}}{\dot{m}_{th}} \tag{1}$$

where $\dot{m}$ is the measured mass flow rate, while $\dot{m}_{th}$ is the maximum theoretical mass flow rate. The latter is defined in Eq.2:

$$\dot{m}_{th} = Z\frac{d_v^2\pi}{4}\rho\sqrt{\frac{2\Delta p}{\rho_m}} \tag{2}$$

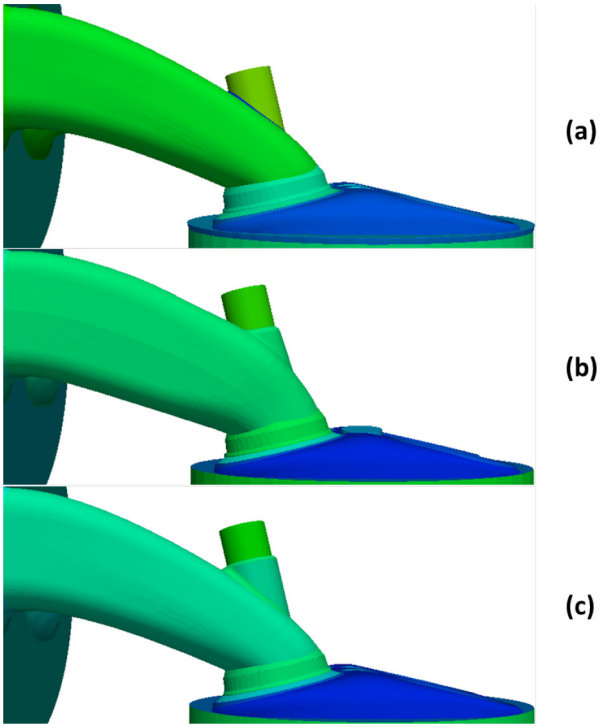

Figure 4. Initial engine head layout (a) and modified geometries (b),(c) on the basis of the provided CFD results

Each term of Eq.2 is reported in Tab.1.

Table 1. Description of the terms of Eq.2

Equation term	Description
Z	Number of valves
d_v	Inner seat diameter
Δp	Pressure drop
ρ and ρ_m	Density and mean density of air

The *TR* was evaluated according to Eq.3:

$$TR = \frac{\omega_{FK}}{\omega_{Mot}} \tag{3}$$

The terms of Eq.3 are:

$$\omega_{FK} = \frac{\sum \omega_i r_i^2 f_i}{\sum r_i^2 f_i} \tag{4}$$

$$\omega_{MOT} = \frac{\pi\bar{v}}{s} \tag{5}$$

where it is:

$$c_m = \bar{v} = \frac{sn}{30} \tag{6}$$

$$\omega = \frac{2n\pi}{60} \tag{7}$$

$$v_i = v_{PIV} - \bar{v} \tag{8}$$

$$\omega_i = \frac{v_i}{r_i} \tag{9}$$

The description of each parameter belonging to the tumble-related equations is reported in Tab.2. In order to compute the *TR* value as reported in Eq.3, a specific function was written and implemented in OF. Each case which will be described in this section was tested under steady-state, un-compressible conditions, with a pressure drop across the valves of 2000 Pa and a RANS *standard k-ε* model for turbulence prediction. Fig.5 shows the results achieved for the layout (a) as a function of the ratio between the valve lift and the valve diameter. Both the trends of c_d and *TR* were satisfactory and provided an output which was in line with what was possible to expect from such intake ports geometry. A subsequent step which was considered by the manufacturer consisted in mantaining an intensity of tumble motion inside the chamber close to what was achieved for the engine layout (a) while, at the same time, increasing the intake mass flow rate, and thus the c_d coefficient. As a consequence, the engine layout (b) of Fig.4 was developed and simulated under the previously described conditions. The main results are shown in Tab.3 as a percentage difference between the new values and what was obtained for the original set-up. It is possible to notice how the goal of reaching a higher mass flow rate value was successfully achieved, even if such a result was obtained at the expense of the tumble intensity in the engine chamber.

Table 2. Parameters of the tumble-related equations

Parameter	Description
c_m	Mean piston velocity
s	Engine stroke
n	Engine speed $[min^{-1}]$
ω_{MOT}	Angular velocity of engine resulting from Eq.6 and Eq.7
$\bar{v}$	Mean axial velocity
ω_{FK}	Angular velocity of solid body rotation corresponding to velocity distribution v_{PIV}
r_i	Cell distance from piston axis
f_i	Cell area

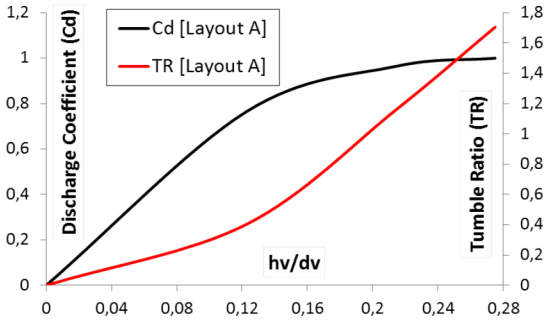

Figure 5. TR and normalized c_d coefficient as functions of the ratio

Table 3. Per cent gap of engine layout (b) c_d and TR coefficients over layout (a) results

$\frac{h_v}{d_v}$	Flow coefficient (c_d)	Tumble Ratio (TR)
0.1224	+3%	−11%
0.214	+6.6%	−19.3%
0.275	+8.3%	−18.6%

The reported reduction of generated tumble inside the cylinder can also be inferred from the velocity glyph analysis displayed in Fig.6. As it is shown in Fig.7, these phenomena are due to intake ports with a higher flow cross sectional area for the second geometry, which direct the flow more axially in the cylinder and less towards the opposite engine walls. Despite the gains in terms of flow coefficient, it was considered unacceptable to have such a decrease in intensity of tumble.

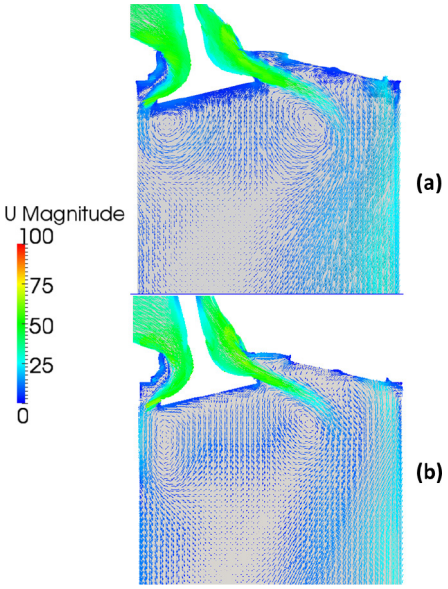

Figure 6. Flow velocity glyph analysis for original (a) and second (b) intake ports configuration with a ratio

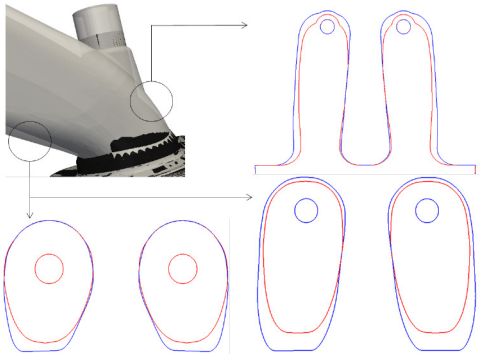

Figure 7. Main differences between the intake geometries of layout (a) [in red] and (b) [in blue]

A third cylinder head set-up (layout (c)) was thus introduced. As it is possible to observe in Fig.8, and making also reference to Fig.4, the layout (c) was designed to be extremely similar to the original one, with only a difference in the region where the valve intake caps connect to the ports. The flow cross sectional area became greater in that zone with the goal to increase the mass flow rate as much as possible, while the shape was kept equivalent to that of the first geometry, in order to avoid the losses in tumble intensity which afflicted the second layout. Computations for the third geometry case were performed with the same numerical set-up as before and Fig.9 shows that a slight increase in both flow coefficient and *TR* was achieved. On the basis of such information, results from the third intake port layout were considered satisfactory enough and this configuration was identified as the reference one.

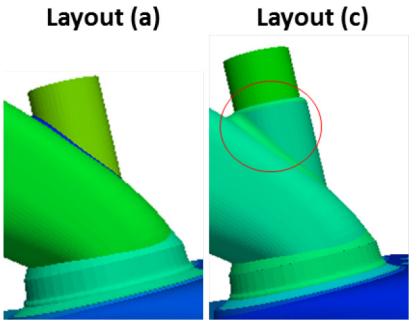

Figure 8. Detail of the increased cross sectional area at the intake caps connection for layout (c) geometry

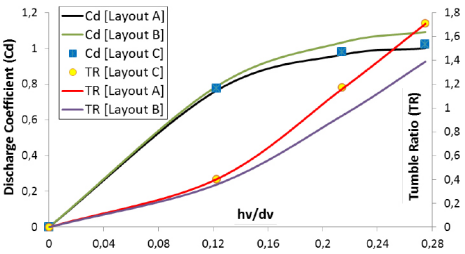

Figure 9. TR and normalized flow coefficient comparison for the three different layouts of the intake ducts

Full-Cycle Cold-Flow Simulations

A subsequent step in the design process was to assess also under transient conditions all the aspects which were observed by means of the steady-state simulations. In particular, the chosen valve lift profile has a high influence on the level of performance and efficiency, as it must guarantee adequate levels of in-cylinder charge flow motion, as well as of turbulence intensity and kinetic energy. Fig.10 shows the intake and exhaust valve lift profile which was tested under the full-cycle simulations. The achievement of high levels of turbulence intensity was deemed as a very important task, given that the engine will also feature an advanced corona discharge ignition methodology. As a consequence, a parameter that was thus specifically evaluated is the ratio between the turbulent fluctuations and the mean piston speed, which is very important at the end of the compression phase since it allows to undertsand whether or not the intake ducts are optimized. The main operating points which were chosen to be tested in accordance with the manufacturer were the full power and the full torque conditions. Furthermore, a focus was also put on the partial load state, since it is the one which presents the highest problems regarding the emissions and the contamination of the fresh charge by the residual gases from the previous engine cycle. The latter phenomenon is especially of high relevance in this case, since the engine is characterized by the presence of an Exhaust Gas Recirculation (EGR) system. The main available details about the operating conditions and the specifications of the engine are reported in Tab.4.

As far as the numerical set-up of the simulations is concerned, a transient, compressible flow approach was chosen, along with second order numerical schemes and a RANS *standard k-ε* model for turbulence. Furthermore, scalable wall-functions were used in order to avoid that too small grid resolutions at the wall boundary close to the valve region could negatively affect the computed turbulence field. The inlet profiles of temperature and total pressure were imposed as a function in time of the crank angle value, and they were provided for each case by 1D calculations executed at TU Graz by means of the AVL BOOST™ ICE simulation software. This approach not only allowed for an accurate initialization of the 3D simulations, but it also served as a validation method for the achieved results, since in-cylinder temperature, pressure and mass profiles for each engine operating condition were provided. The main specifications about the calculations (starting point, time-step and number of simulated engine cycles) are also reported in Tab.4.

Table 4. Main details about operating conditions, engine specifications and numerical set-up

Parameter	Value
Bore	0.135 m
Stroke	0.15 m
Compression ratio	∽ 13
Number of valves	4
Operating point	**Description**
Full load	Maximum power @1900 rpm
Full torque	Maximum torque @1000 rpm
Partial load	100 kW @1200 rpm
Parameter	**Description**
Starting point of the simulations	335 °CA
Average time-step of the simulations	0.005 °CA
Number of simulated engine cycles for each case	1

The first case to be simulated has been the full-load one, for which a validation assessment of the *Flow Coefficient* (c_d) was initially performed, according to the methodology previously described for the steady-state simulations. The purpose of such a choice was to verifiy the consistency of the achieved intake mass flow rate, for different values of valve lift, with what was obtained from the flow bench computations. The results are shown in Fig.11. The black curve represents the c_d coefficient for the first intake ducts geometry (engine layout (a)); the red dots are the values achieved with steady-state simulations for the layout (c) configuration; finally, the green dots represent the c_d values which were achieved for the 1900 rpm cold-flow computation, while the light blue curve stands for the correspondent engine °CA position. As it can be noticed, the outcome from the full-cycle simulation fits the data trend derived from the steady-state approach. In particular, the valve closing phase shows a good agreement with the flow bench results.

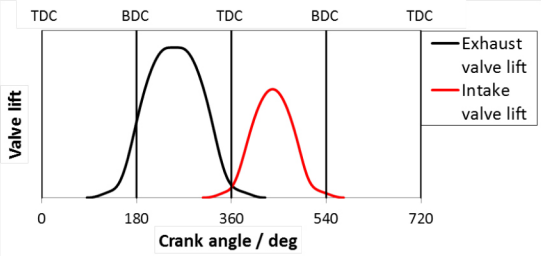

Figure 10. Valve lift Profile A adopted for the cold-flow simulations

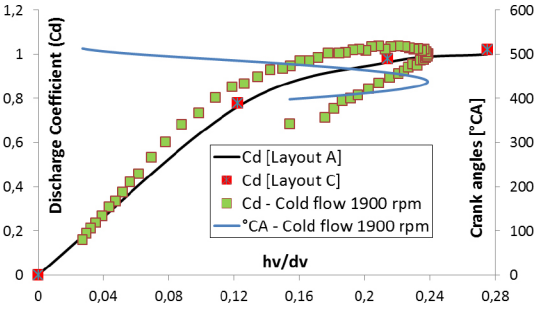

Figure 11. Normalized flow coefficient comparison between steady-state and 1900 rpm cold-flow simulations

Fig.12 reports glyphs of the velocity coloured by its magnitude and it shows that there is a good qualitative agreement between the computed in-cylinder flow respectively of the steady-state flow bench simulation and the full-load cold-flow. For both cases, the main tumble vortices which are visible on the right side of the intake valve are consistent in direction, while the smaller vortex shown on the left side of the valve, which was captured by the flow bench computation, is visible as well for the cold-flow case. Furthermore, the interaction of the two described vortices with the in-cylinder charge also results very well predicted and consistent, since it is possible to notice how, for both cases, it leads to a flow recirculation zone under the intake valve. Finally, the higher velocity magnitude for the full-cycle case compared to the steady-state condition is due to a higher pressure drop between the intake ports and the cylinder.

The *Tumble Ratio (TR)* of the in-cylinder charge for the full-cycle simulations has been evaluated according to the methodology proposed by [13]. On the basis of such approach, the TR is defined as the ratio of the equivalent solid-body angular speed to the engine speed, and it is calculated from the mean velocity distribution in the central symmetry plane on the basis of Eq.10:

$$TR = \frac{\sum_{i=1}^{n}\sum_{j=1}^{m}(\vec{r}_{i,j} - \vec{r}_c) \times \vec{V}_{i,j}}{\omega \sum_{i=1}^{n}\sum_{j=1}^{m}(\vec{r}_{i,j} - \vec{r}_c) \cdot (\vec{r}_{i,j} - \vec{r}_c)} \quad (10)$$

The term $(\vec{r}_{i,j} - \vec{r}_c)$ represents the distance of a specific position *(i,j)* from the center of rotation, with the index *i* referring to the x direction and *j* to the y direction, while ω is the angular speed of the engine and $\vec{V}_{i,j}$ is the velocity in the reference position. According to such a definition, the TR is a vector which is perpendicular to a plane parallel to the cylinder axis, while the center of rotation is assumed to be equal to the centroid of the cylinder symmetry plane. Since the engine topology changes with time, the position of the centroid changes as well, by shifting upwards or downwards along with the movement of the piston.

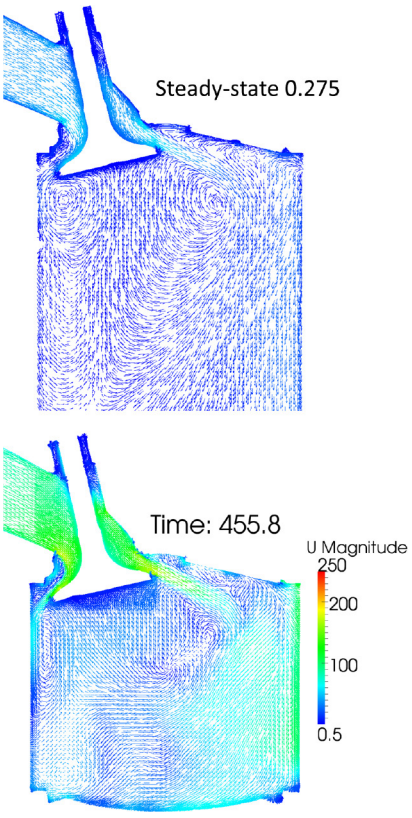

Figure 12. Charge flow motion comparison between the steady-state condition for the set-up (a) and the 1900 rpm cold-flow simulation (b)

Fig.13 displays the TR trend for the full-load and partial load engine operating conditions. In both cases the behavior of the curve results to be consistent with what was achieved by Lucchini et al. [27] in previous full-cycle simulations for GDI engines. Both the TR trends show a peak during the intake phase, a decrease and then another peak of lower intensity before the end of the compression phase. With reference to the full-load operating condition, the reasons behind the TR reduction which takes place between the two peaks are described in Fig.14 and Fig.15. The phenomenon is due to an interaction between different flow vortices that rotate with opposite directions,

interacting with each other until the intensity of one of them prevails during the evolution over time of the in-cylinder charge flow. At 420.5 °CA the intake valves are opening and the main charge flow (**green circle**) is entering the chamber, with a deployed TR of around 0.75. Subsequently, the intake phase continues and the TR reaches its maximum peak around the 445 - 465 °CA range, with the secondary flow on the left side of the valve (**red circle**) increasing in its intensity as well at 461.2 °CA, also due to the expansion movement of the piston. Once the intake valves are closed, not only the main flow structure reaches the piston (482.8 °CA, (**black circle**)), but it also begins to interact with the secondary flow, creating two opposite charge vortices (502.6 °CA, (**1 - 2**)). Furthermore, a third vortex (502.6 °CA, (**3**)) is generated by another interaction between the secondary flow and the fraction of primary flow which previously reached the piston. Such a complex interaction between different in-cylinder motions leads to the condition shown for the 542.8 °CA value for which, with the piston reaching its bottom dead center position, in the cylinder there are only two vortices that are both subjected to low values of velocity magnitude and possess opposite direction ((**2 - 3**)). As a consequence, the TR reaches its lowest intensity. Finally, when the piston is moving upwards (621.1 °CA), vortex number **2** gets destroyed, while on the contrary vortex **3** is enhanced, then it moves towards the right side of the engine domain and it is conserved up to the end of the compression phase. This behavior explains the subsequent increase of TR which ends with the achievement of the second peak around 50-70 °CA before the piston top dead center position. It must furthermore be noticed how all the three engine operating conditions display very close values of TR in magnitude. Such a fact confirms how the TR is heavily influenced by the adopted intake valves lift law, which, as previously reported, was chosen to be the same for every full-cycle, cold-flow simulation proposed in this work.

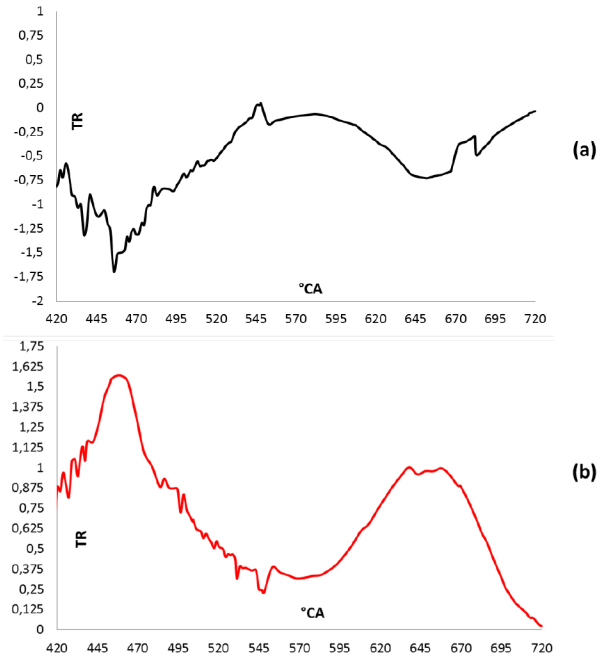

Figure 13. TR trend for the full-load 1900 rpm (a) and the partial load 1200 rpm (b) simulations

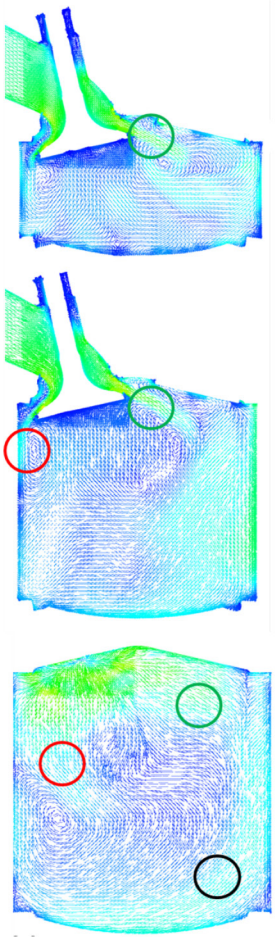

Figure 14. Charge motion analysis for different °CA positions (420.5 - 461.2 - 482.8), 1900 rpm full-load case

Fig.16 and Fig.17 respectively report the comparative analysis of the turbulent kinetic energy (TKE) and the ratio of the turbulent fluctuations over the mean piston speed ($\frac{u'}{U_p}$). The latter is calculated according to Eq.11:

$$U_p = \frac{2sn}{60} \tag{11}$$

As it was possible to expect, the TKE heavily depends on the engine speed, with thus the 1000 rpm operating point showing the lowest intensity of turbulent fluctuations. However, the trend of the curves is equal for each one of the tested cases and it shows the influence of the adopted valve lift Profile A, since the same behavior which was observed for the TR is noticeable. As a conclusive note to this analysis, with reference to Fig.18 (related to a 700 crank angle position), it is worth noticing that, for each tested operating condition, the ($\frac{u'}{U_p}$) ratio always assumes a value equal or greater than 0.5 towards the end of the compression phase. Such a result is very important, since according to what is reported in literature [28, 29], it

means that the engine is characterized by optimized intake ducts, while a value around 0.2 is considered to be the standard for non-optimized engines.

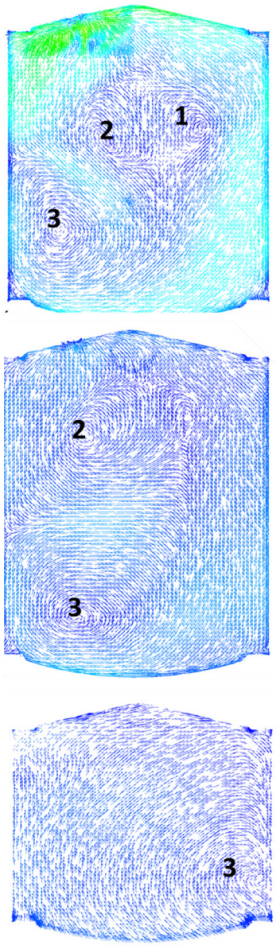

Figure 15. Vortices analysis for different °CA positions (502.6 -542.8 - 621.1) towards TDC, 1900 rpm full-load case

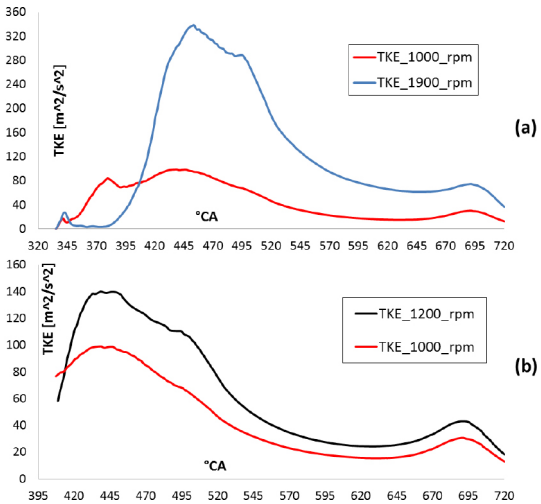

Figure 16. Trends of turbulent kinetic energy (TKE)

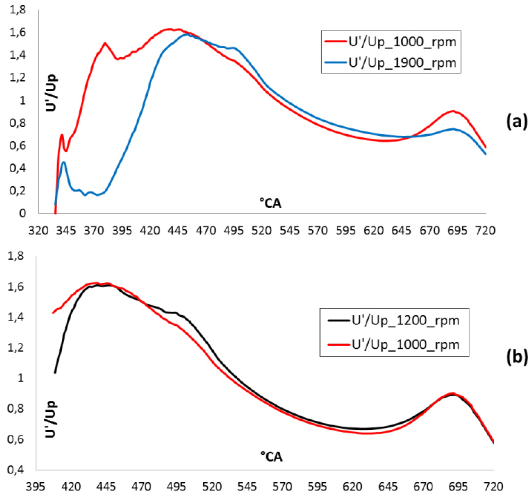

Figure 17. Trends of the ratio between the turbulent fluctuations and the mean piston speed

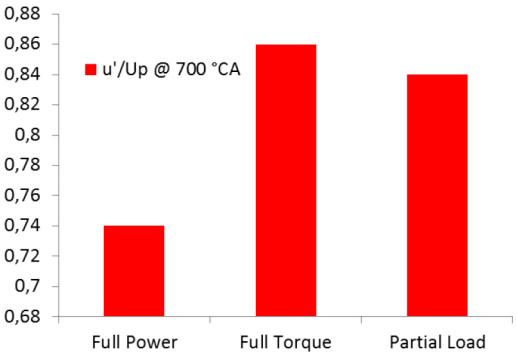

Figure 18. Comparison of the turbulent fluctuations-mean piston speed ratio for each of the simulated engine operating conditions

Full-Cycle Simulations with Gaseous Injection

Recent studies performed on DI, NG heavy-duty engines [30] demonstrated the importance of an optimized EGR value for each operating condition, since it allows for a reduction of NO_x emissions as well as for a better knock control. Another aspect of high importance is the air-fuel mixing process, which for a DISI engine is required to lead to the formation of a highly homogeneous mixture. As a consequence, the main parameters which were evaluated in this work are the influence of the injected gas over the charge flow motion, in terms of both TR and TKE, and in terms of the efficiency of the air-fuel mixing process. Different EGR values for different engine operating conditions were tested, and the simulations were also performed by considering multiple valve lift laws, both in order to take into account their effect on the mixing and to gather useful data for a possible application of a variable valve timing approach. The main conditions which were tested are:

1. The partial load, 1200 rpm operating point, which was described in the previous section of this paper;
2. The 1300 rpm operating point, corresponding to a brake mean effective pressure (BMEP) of 2 bar. A second valve lift law (Profile B) was adopted for this case. Different start of injection (SOI) timings were tested for this configuration;

3. The 1900 rpm, full-load condition with a third valve lift law (Profile C);
4. The 1900 rpm, full-load condition with a fourth valve lift law (Profile D).

Natural gas with a volume fraction of 84.7% in methane was used as reference fuel for each computation. Fig.19 shows the differences between the adopted valve lift laws with reference to the intake profiles, while Tab.5 reports the most important parameters regarding the full-cycle simulations with fuel injection. Regarding the injector, natural gas is injected by a centrally mounted multi-hole nozzle with a pressure of approximately 20 bar. Moreover, the layout of the injector is similar to solutions recently studied in other works [16].

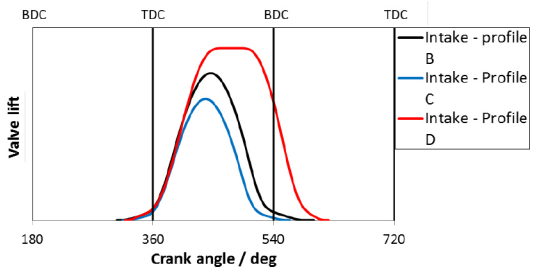

Figure 19. Differences between the intake valves profiles adopted for the full-cycle simulations with fuel injection

Table 5. Main parameters for the full-cycle simulations with fuel injection

Operating condition	SOI
Partial load 1200 rpm	423.8 °CA
1300 rpm, 2 bar BMEP	423.8-444 °CA
Full load 1900 rpm, Profile C	413 °CA
Full load 1900 rpm, Profile D	413 °CA

Modeling the injection of supersonic gas can result in a high effort in terms of resources even for cases with simple computational domains, therefore coupling it with a full-cycle simulation in a complex geometry represents a very challenging task. Concerning the computational mesh, to ensure a good compromise between the accuracy of results and the required computational time, the same grid structure of the cold-flow simulations was retained, with an additional refinement in the region where the fuel is injected. As it is shown in Fig.20, an internal refinement of 0.25 mm was adopted in the region immediately below the injector nozzles, while the injector walls were refined up to 0.125 mm and the cell size of the internal grid for the injector channels was set equal to 0.0625 mm. A complete, transient simulation of the sole injection process is not compatible with a whole full-cycle computation in terms of time and length scales. As a consequence, after that an in-depth analysis of all the viable alternatives was carried out by all the project partners, a specific approach was identified to be the best compromise.

According to such a choice, a complete, transient CFD simulation of the injection phase has been performed by the injector supplier and the achieved average pressure, temperature and velocity fields at the nozzle holes were subsequently used as boundary conditions for the subsequent full-cycle simulations.

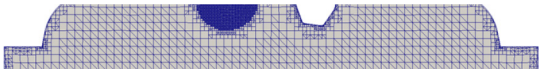

Figure 20. Focus on the internal mesh refinement for the zone below the injector nozzle holes

As far as the set-up of the calculations is concerned, numerical schemes and turbulence model were not changed from the cold-flow simulations. Once more, the inlet profiles of temperature and total pressure were imposed as a function in time of the crank angle values and they were provided for each case by 1D calculations performed at TU Graz by means of the AVL BOOST™ ICE simulation software.

The efficiency of the air-fuel mixing process was evaluated in terms of:

1. Relative air-fuel ratio *Lambda*, defined as

$$Lambda = \frac{\left(\frac{m_{air}}{m_{fuel}}\right)}{\left(\frac{m_{air}}{m_{fuel}}\right)\Big|_{Stoichiometric}} \tag{12}$$

   Since each case was simulated under stoichiometric conditions, Lambda was always expected to be unitary at the end of the intake and injection phases. The stoichiometric air-fuel ratio resulted to be equal to 15.46 from the adopted natural gas composition;
2. The *Equivalence Ratio (ER)*, expressed as the inverse of the relative air fuel ratio;
3. The *Homogeneity Index (HI)*, which is defined as

$$HI = 1 - \frac{\sigma}{\sigma_{n,h}} \tag{13}$$

   where σ is the standard deviation of fuel mass fraction and $\sigma_{n,h}$ is the standard deviation under completely inhomogeneous conditions (fuel not mixed with air). $\sigma_{n,h}$ is computed as

$$\sigma_{n,h} = \frac{\sqrt{\frac{A}{F}}}{\left(1 + \frac{A}{F}\right)} \tag{14}$$

   where ther terms A and F respectively represent the mass of air and fuel.

Results for the partial load case are summarized in Fig.21, where the evolution of tumble ratio, turbulent kinetic energy and homogeneity index is reported for the simulations performed with and without fuel injection.

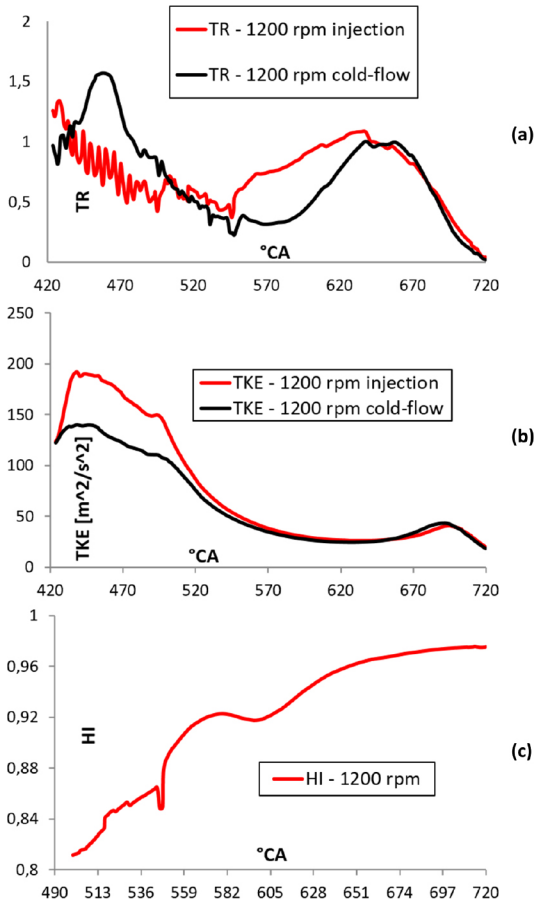

Figure 21. Partial load, 1200 rpm cases with and without injection, TR (a), TKE (b) and HI (c)

As it is possible to notice in Fig.21(a), the tumble motion of the flow charge is significantly affected by the injection process, with the expected peak of TR which gets destroyed by the strong interaction between the injected fuel jet and the in-cylinder charge motions. This fact reflects into a subsequent increase of tumble for the range between 550 and 650 °CA, immediately after the end of the injection. Finally, towards the end of the compression phase, the two curves are shown to be nearly coincident. Fig.21(b) demonstrates that there is an expected increment of TKE during the injection phase, which is due to the contribution of the high pressure fuel that is injected into the engine chamber. Once the injection stops, the TKE values of both cases become very similar. Fig.21(c) reports the trend of the HI as a function of the crank angle value: it is possible to notice how the air-fuel homogeneity gradually increases during the injection, then it has a sudden increment of slope during the transient closure of the injector before almost reaching an unitary value towards the end of the compression phase. This described trend for the HI is consistent with what was observed in previous works [27], furthermore such a relatively high homogeneity index value is encouraging since it is generally related to:

1. High combustion efficiency;
2. Reduced cyclic variability;
3. Reduced emissions (soot, NO_x, CO) due to the presence of very rich or very lean regions.

A sensitivity analysis was performed for the 1300 rpm, 2 bar BMEP operating condition as a function of the SOI value, and its main results are shown in Fig.22. This case was chosen because it had the lowest amount of fuel to be injected, thus resulting the less demanding operating point in terms of computational time and resources.

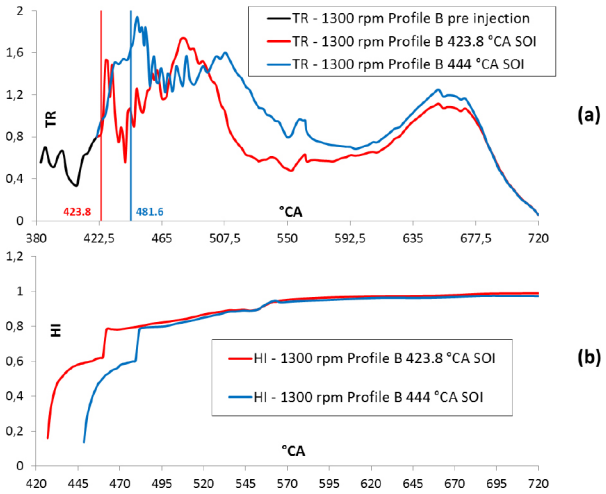

Figure 22. TR (a) and HI (b) results for the 1300 rpm operating point, for two values of injection SOI

Fig.22(a) reports the obtained trends of TR. The case with SOI of 444 °CA demonstrates, both on average and as a peak, considerably higher values of TR if compared to the 423.8 °CA set-up. The delayed injection timing seems thus to exert less destructive impact on the tumble flow motion of the fresh charge, both during and after the injection phase. Fig.22(b) reports the HI trends, which result to be very similar for both cases. Indeed, after the abrupt increase of mixture homogeneity at the end of the injection, they keep on increasing during the compression phase up to almost unitary values. Moreover, on the basis of a more focused analysis it is possible to notice that the final HI value for the 423.8 °CA results to be slightly higher. This observed behaviour was expected, since it is a consequence of the higher amount of time which is available for the mixing process of air and fuel.

Fig.23(a) compares the trends of TR for the Profile C and Profile D valve timings in relation to the 1900 rpm full load operating point. It can be observed that the Profile D allows for a significantly higher tumble intensity to be generated inside the chamber during the intake phase. Such a behavior happens because the Profile D lift law is characterized by an extended time interval during which the intake valves are fully open, furthermore reaching the highest peak of lift between all the tested configurations. The Profile C, on the other hand, is much closer to the others tested before, indeed its TR trend is much more consistent with what was reported in the previous sections of this work, displaying the highest peak during the intake, a decrease, and a second, albeit lower, peak during the compression phase. Fig.23(b) reports the effects of the two different valve lift profiles on the HI for the full-load condition. As Lambda reaches its stoichiometric value during the fuel injection, the HI always gradually increases as it happens for the partial load. Once the injection stops, there is a large increase in the mixture homogeneity, then the HI starts to gradually rise again almost to unity. Fig.23(c)

shows the probability mass function (PMF) of Lambda, calculated for the Profile D case at 720 °CA. As expected from the stoichiometric conditions, most of the mixture is found inside the cylinder with lambda values close to one, fact that will make it possible to ensure a stable combustion process even at full power conditions, which is the case for which the longest injection duration is expected.

The accuracy of the results for the 1900 rpm Profile D case was validated against the 1D data in terms of cylinder pressure and captured mass, as it is respectively shown in Fig.24(a) and (b). In-cylinder pressure profiles are very similar until the end of the compression phase, where the difference is explained by the fact that CFD simulations do not account for the start of combustion. Fig.24(b) shows the rather good agreement in computed cylinder mass between 1D and 3D results until 600 °CA. Afterwards, a sensible difference was found, since during the gas exchange process 1D simulations do not account for the gaseous fuel injection, which however seems to be responsible for a reduction of the volumetric efficiency. A partial backflow of fresh air and recirculated gases through the intake ducts is predicted by both 1D and 3D computations, while the latter also account for a loss in fuel mass. The discrepancy in terms of trapped mass between the two reported curves does not thus represent a problem of accuracy for the 3D simulations, but it is a consequence of the different density of the in-cylinder mass which is due to the presence of fuel. This state also led the mixture to behave differently during the backflow phase and, overall, the loss in fuel computed by CFD simulations allowed to understand the need to account for a reduction of around 4% in mass of fresh charge, in order to guarantee the required stoichiometric operating condition.

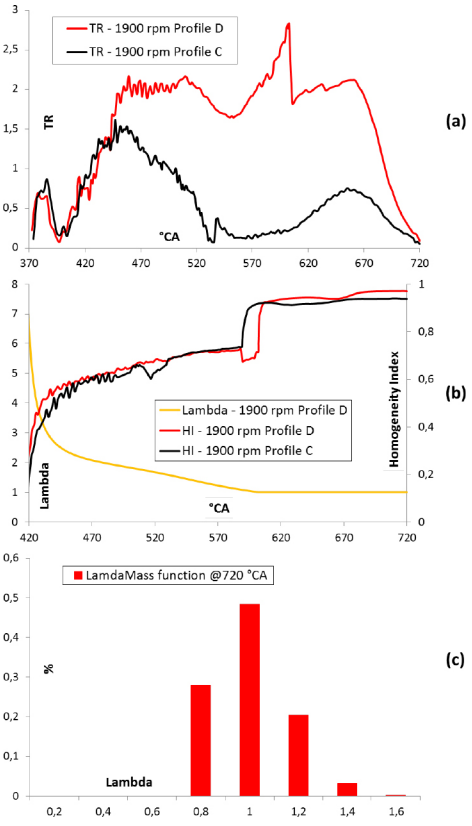

Figure 23. 1900 rpm injection results, comparison of TR (a), HI (b), and Lambda probability mass function (c) at 720 °CA for the Profile D case

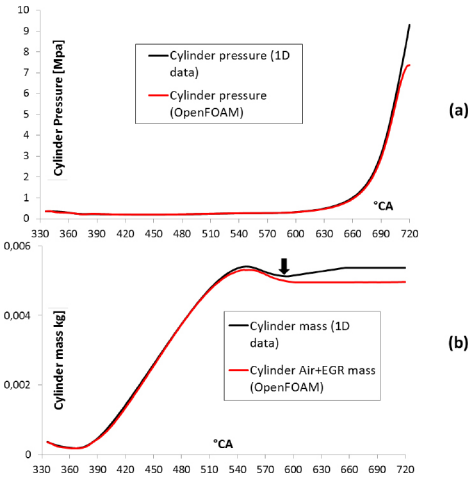

Figure 24. Validation of the 1900 rpm Profile D results against 1D data for cylinder pressure (a) and captured mass (b)

Fig.25 reports the distribution of in-cylinder equivalence ratio, for the 1900 rpm Profile D case, on two orthogonal planes passing through the spark-plug location during the compression stroke. An almost homogeneous mixture with equivalence ratio equal to 1.0 was found close to the spark-plug, thus increasing the efficiency of the ignition process. However, it is possible to distinguish the presence of relatively lean zones located close to the cylinder liner and rich zones close to the piston. The first ones might lead to formation of unburned hydrocarbons while the second ones can lead to CO formation. However, the high levels of in-cylinder turbulence are expected to enhance the mixing between burned gases with a potential positive effect on CO and HC oxidation.

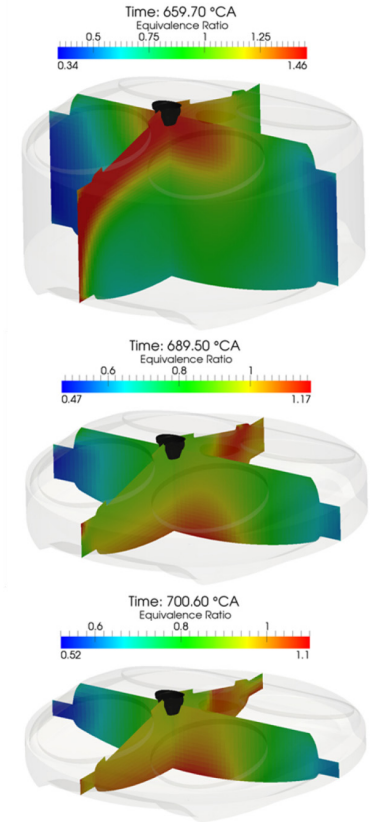

Figure 25. Distribution of in-cylinder equivalence ratio on two orthogonal planes passing through the spark-plug location, during the compression stroke, for the 1900 rpm Profile D simulation

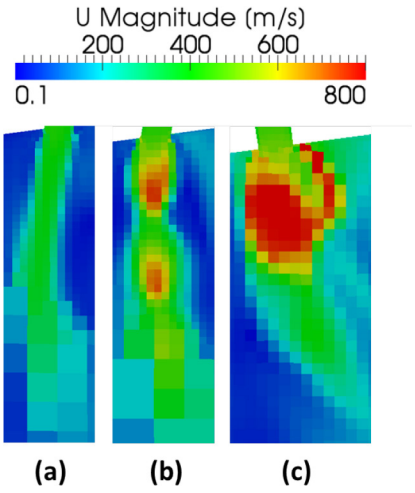

Figure 26. Underexpanded supersonic gaseous jet analysis for different values of the ratio between injection and engine chamber pressure

As a conclusive step, an analysis of the characteristics of the underexpanded jet flow was performed, since while it is true that the previously described engine-related parameters are what hold the highest importance due to the nature itself of the project, the work nevertheless provided the opportunity to assess that the most important thermo-physical aspects of supersonic gaseous flows could still be captured even with a CFD set-up which has overall been thought in order to best suit the schedule and the computational requirements of an industrial-oriented project. When a supersonic gas is discharged from a high pressure nozzle it becomes subjected to a phenomenon of underexpansion which is characterized by complex instabilities that are dependent on the ratio between the pressure of the gas and that of the chamber. When the jet is exhausted from the nozzle, it expands up to the jet boundary, which is the flow interface characterized by a condition of ambient pressure. As a consequence, the interaction between the wave and the boundary reflects the expansion wave as a compression one, with the cyclic repetition of this phenomenon leading to the accumulation of the waves, thus generating the so called barrel shock. For high values of pressure ratio, the latter interacts with another shock which is normal to the jet axis, leading to the Mach Disk effect, for which an abrupt decrease of the jet velocity is observed. However, such process does not happen for lower values of pressure ratio, with the jet flow that is thus subjected to the wave expansion and compression effects even downstream of the injector nozzle [31, 32]. The described jet behavior is observable in Fig.26, which respectively reports a low pressure injection event in a high pressure chamber (Fig.26(a), full power operating point, side channels of the injector which work at lower pressure compared to the middle one), a high pressure injection event in a high pressure chamber (Fig.26(b), full power operating point, middle injector nozzle) and finally a high pressure injection event in a low pressure chamber (Fig.26(c), partial load operating point, middle injector nozzle, highest simulated pressure ratio). Fig.26(a) reports a barrel shock formation which is characterized by expansion and compression waves of low intensity, given the high pressure in the chamber and the low value of injection pressure. Fig.26(b) shows the same phenomenon but for a higher value of injection pressure, so that it is possible to notice the greater effects of expansion and subsequent compression on the velocity magnitude of the gas. Finally, Fig.26(c) displays the case for which the pressure ratio is greater than the minimum value which is necessary to lead to the formation of the Mach Disk. Such analysis confirmed that, while the mesh and the numerical set-up were primarily thought as the best compromise between accuracy and minimum requirements of computational resources, it still resulted possible to capture the most important physical details of a gas flow injected at supersonic velocities.

Conclusions

CFD simulations were carried out in the context of the HDGas project to support the design and the development process of a natural gas, direct injection engine. The calculations were performed with the OpenFOAM software coupled with the LibICE, and they successfully supported the following activities:

1. Design of the intake ports, by identifying a configuration with the best compromise in terms of tumble ratio and flow coefficient;
2. Verification of the intake ports behavior during the simulation of the gas exchange and compression phases. The proposed layout resulted capable to generate the proper amount of turbulence for the different tested operating conditions;
3. Detailed study of the air-fuel mixing process, including the injection of natural gas. Under the different analyzed conditions it was possible to verify that the proposed injector configuration properly distributes the fuel inside the cylinder, and that the adopted value of injection mass flow rate allows for the delivery of the proper amount of fuel, even under full load operating conditions.

The activities carried out within this work package thus allowed to analyze in detail many aspects related to the intake, injection and combustion systems design of a modern direct-injection, natural gas engine. Finally, a conclusive analysis of the thermophysical behavior of the injected fuel assessed the capability of the adopted numerical setup to capture the most important physical details related to the underexpanded supersonic jets, thus showing a compromise between a satisfying accuracy of the results and an adequate demand of computational resources.

References

1. Cho H.M. and He B.Q.. Spark ignition natural gas engines - a review. energy conversion and management. 48(2), 608-618, 2007.
2. Verhelst, S., Sierens, R., and Verstraeten, S., "A Critical Review of Experimental Research on Hydrogen Fueled SI Engines," SAE Technical Paper 2006-01-0430, 2006, doi:10.4271/2006-01-0430.
3. White C.M., Steeper R.R., and Lutz A.E.. The hydrogen-fueled internal combustion engine: a technical review. *Int. J. Hydrogen Energy*, 31:1292-1305, 2006.
4. Obermair, H., Scarcelli, R., and Wallner, T., "Efficiency Improved Combustion System for Hydrogen Direct Injection Operation," SAE Technical Paper 2010-01-2170, 2010, doi:10.4271/2010-01-2170.
5. d'Ambrosio, S., Spessa, E., Vassallo, A., Ferrera, M. et al., "Experimental Investigation of Fuel Consumption, Exhaust Emissions and Heat Release of a Small-Displacement Turbocharged CNG Engine," SAE Technical Paper 2006-01-0049, 2006, doi:10.4271/2006-01-0049.

6. Soltic, P., "CO2 Reduction and Cost Efficiency Potential of Natural Gas Hybrid Passenger Cars," *SAE Int. J. Engines* 4(2):2395-2404, 2011, doi:10.4271/2011-24-0110.
7. Korakianitis T., Namasivayam A.M., and Crookes R.J.. Natural gas fueled spark ignition (si) and compression-ignition (ci) engine performance and emissions. *Progress in Energy and Combustion Science*, 37:89-112, 2011.
8. Kalam M.A. and Masjuki H.H.. An experimental investigation of high performance natural gas engine with direct injection. *Energy*, vol. 36, pp. 3563-3571, 2011.
9. Verhelst S. and Wallner T.. Hydrogen-fueled internal combustion engines. *Progress in Energy and Combustion Science*, Vol. 35, 490-527, 2009.
10. Andreassi L., Cordiner S., Mulone V., Reynolds C., and Evans R.. Numerical-experimental comparison on the performance of a partially stratified charge natural gas fueled engine. ASME, Internal Combustion Engine Division Fall Technical Conference, 2004.
11. Xu B.P., Zhang J.P., Wen J.X., Dembele S., and Kar-watzki J.. Numerical study of a highly under-expanded hydrogen jet. International Conference on Hydrogen Safety, Pisa, Italy, September 2005.
12. White T.R. and Milton B.E.. Shock waves. 18:353, 2008.
13. Scarcelli R., Wallner T., Obermair H., Salazar V.M., and Kaiser S.A.. Cfd and optical investigations of fluid dynamics and mixture formation in a di-h2 ice. *ASME*, ICEF2010-35084, 2010.
14. Scarcelli R., Kastengren A.L., Powell C.F., Wallner T., and Matthias N.S.. High-pressure gaseous injection: a comprehensive analysis of gas dynamics and mixing effects. Proceedings of the Internal Combustion Engine Division - Fall Technical Conference, ICEF2012-92137, 2012.
15. Baratta, M., Rapetto, N., Spessa, E., Fuerhapter, A. et al., "Numerical and Experimental Analysis of Mixture Formation and Performance in a Direct Injection CNG Engine," SAE Technical Paper 2012-01-0401, 2012, doi:10.4271/2012-01-0401.
16. Bartolucci, L., Scarcelli, R., Wallner, T., Swantek, A. et al., "CFD and X-Ray Analysis of Gaseous Direct Injection from an Outward Opening Injector," SAE Technical Paper 2016-01-0850, 2016, doi:10.4271/2016-01-0850.
17. Lucchini, T., D'Errico, G., Brusiani, F., Bianchi, G. et al., "Multi-dimensional modeling of the air/fuel mixture formation process in a PFI engine for motorcycle applications," SAE Technical Paper 2009-24-0015, 2009, doi:10.4271/2009-24-0015.
18. Lucchini, T., D'Errico, G., and Fiocco, M., "Multi-Dimensional Modeling of Gas Exchange and Fuel-Air Mixing Processes in a Direct-Injection, Gas Fueled Engine," SAE Technical Paper 2011-24-0036, 2011, doi:10.4271/2011-24-0036.
19. Montanaro, A., Allocca, L., Ettorre, D., Lucchini, T. et al., "Experimental Characterization of High-Pressure Impinging Sprays for CFD Modeling of GDI Engines," *SAE Int. J. Engines* 4(1):747-763, 2011, doi:10.4271/2011-01-0685.
20. Lucchini, T., D'Errico, G., Onorati, A., Bonandrini, G. et al., "Development of a CFD Approach to Model Fuel-Air Mixing in Gasoline Direct-Injection Engines," SAE Technical Paper 2012-01-0146, 2012, doi:10.4271/2012-01-0146.
21. Lucchini, T., Della Torre, A., D'Errico, G., Montenegro, G. et al., "Automatic Mesh Generation for CFD Simulations of Direct-Injection Engines," SAE Technical Paper 2015-01-0376, 2015, doi:10.4271/2015-01-0376.
22. Bartolucci, L., Cordiner, S., Mulone, V., Rocco, V. et al., "Partially Stratified Charge Natural Gas Combustion: A LES Numerical Analysis," SAE Technical Paper 2015-01-0398, 2015, doi:10.4271/2015-01-0398.
23. Bartolucci, L., Cordiner, S., Mulone, V., Rocco, V. et al., "Partially Stratified Charge Natural Gas Combustion: The Impact of Uncertainties on LES Modeling," SAE Technical Paper 2015-24-2409, 2015, doi:10.4271/2015-24-2409.
24. Lucchini, T., D'Errico, G., Jasak, H., and Tukovic, Z., "Automatic Mesh Motion with Topological Changes for Engine Simulation," SAE Technical Paper 2007-01-0170, 2007, doi:10.4271/2007-01-0170.
25. Lucchini T., D'Errico G., Brusiani F., and Bianchi G.. A finite-element based mesh motion technique for internal combustion engine simulations. COMODIA 2008, MS2-3, 2008.
26. Sevik, J., Pamminger, M., Wallner, T., Scarcelli, R. et al., "Performance, Efficiency and Emissions Assessment of Natural Gas Direct Injection compared to Gasoline and Natural Gas Port-Fuel Injection in an Automotive Engine," *SAE Int. J. Engines* 9(2):1130-1142, 2016, doi:10.4271/2016-01-0806.
27. Lucchini, T., Fiocco, M., Onorati, A., Montanaro, A. et al., "Full-Cycle CFD Modeling of Air/Fuel Mixing Process in an Optically Accessible GDI Engine," *SAE Int. J. Engines* 6(3):1610-1625, 2013, doi:10.4271/2013-24-0024.
28. Heywood J.B.. *Internal Combustion Engine Fundamentals*. McGraw-Hill, 1988.
29. Ferrari G.. *Motori a Combustione Interna*. Edizioni Il Capitello, 2001.
30. Zoldak, P. and Naber, J., "Spark Ignited Direct Injection Natural Gas Combustion in a Heavy Duty Single Cylinder Test Engine - AFR and EGR Dilution Effects," SAE Technical Paper 2015-01-2808, 2015, doi:10.4271/2015-01-2808.
31. Irie T., Yasunobu T., Kashimura H., and Setoguchi T.. Characteristics of the mach disk in the underexpanded jet in which the back pressure continuously changes with time. *J. of Thermal Science Vol.*12, *No.*2.
32. Müller, F., Schmitt, M., Wright, Y., and Boulouchos, K., "Determination of Supersonic Inlet Boundaries for Gaseous Engines Based on Detailed RANS and LES Simulations," *SAE Int. J. Engines* 6(3):1532-1543, 2013, doi:10.4271/2013-24-0004.

Contact Information

PhD student Davide Paredi
Department of Energy, Politecnico di Milano
Via Lambruschini, 4
20156 Milano, Italy
davide.paredi@polimi.it

Acknowledgements

The results proposed in this paper were achieved thanks to fundings with Grant from UE, n. 653391, HDGas project.

The Engineering Meetings Board has approved this paper for publication. It has successfully completed SAE's peer review process under the supervision of the session organizer. The process requires a minimum of three (3) reviews by industry experts.

ISSN 0148-7191

http://papers.sae.org/2017-24-0026